Available online at www.sciencedirect.com
SCIENCE DIRECT®
Journal of Chromatography B, 790 (2003) 115–129
JOURNAL OF CHROMATOGRAPHY B
www.elsevier.com/locate/chromb

Direct observation of intraparticle equilibration and the rate-limiting step in adsorption of proteins in chromatographic adsorbents with confocal laser scanning microscopy

Volker Kasche[a,*], Michael de Boer[a], Cesar Lazo[b], Moustafa Gad[a]

[a]*Biotechnology II, TU Hamburg–Harburg, Denickestrasse 15, D-21071 Hamburg, Germany*
[b]*Chemical Engineering, TU Hamburg–Harburg, Eissendorfer Strasse 38, D-21071 Hamburg, Germany*

Abstract

The adsorption of different proteins in a single biospecific and hydrophobic adsorbent particle for preparative protein chromatography has been observed directly by confocal laser scanning microscopy as a function of time at a constant bulk concentration c_b. The bulk concentration was in the non-linear part of the adsorption isotherm. At all times the concentration of free protein at the particle surface was almost equal to the bulk content indicating that external mass transfer resistance is not rate limiting for the adsorption under these conditions. Inside the particles a distinct maximum in adsorbed and free protein concentration that moved inside to a distance of ≈0.2 R (R particle radius) from the particle surface, was observed. This is due to a decreasing solid-phase density and adsorptive capacity in the particle between 0.8 R and R indicating that the fraction of macropores (or void space) is larger in the outer than in the inner part of the adsorbent particles. By increasing the bulk concentration by a factor of 10 the equilibration time was reduced by about the same magnitude. This is in agreement with the concentration dependence of the effective pore diffusion coefficient $D_{p,eff} = D_p/\{\epsilon_p[1 + nK/(K + c)^2]\}$ derived from the mass conservation relations describing the adsorption process. The time dependence protein adsorption up to ≈90% of the equilibration value q^* could be described by a bilinear free driving force model. The rapid equilibration in the outer part of the particle with a half-life time of ≈100 s in the studied systems accounted for 0.3–0.4 q^*. The slower equilibration with a up to ten times longer half-life time, was the adsorption in the inner part of the particle that outside 0.5 R accounts for 0.5–0.6 q^*. These data were compared with literature data for batch adsorption of proteins in biospecific, hydrophobic and ion-exchange adsorbents. They could also be described by a bilinear free driving force model, with about the same quantitative results as obtained for similar conditions in the single particle experiments. The static adsorption parameters, maximum binding site concentration n, and dissociation constant for the protein binding to a binding site K, were determined from Scatchard plots. For the same protein–adsorbent system the plots changed from linear to non-linear with increasing n. This change occurred when the average distance between adjacent binding sites become of the same order of magnitude as the size of the binding site or adsorbed protein. This causes a shielding of free binding sites increasing with n and the concentration of adsorbed protein, yielding a concentration dependence in K. These results show that for a high throughput and rapid adsorption in preparative chromatography, the adsorption step should be carried out in the non-linear part of the adsorption isotherm with concentrations up to c_b where $q^*/c_b \geq 10$ to obtain high protein recoveries. To avoid tailing due to the flow of adsorbed proteins in the inner part of the particles further into the particles at the start of the desorption, and to speed up desorption rates, protein adsorption in the particle within 0.5 R from the particle center should be avoided. This

*Corresponding author. Fax: +49-404-2878-2127.
E-mail address: kasche@tu-harburg.de (V. Kasche).

1570-0232/02/$ – see front matter © 2002 Elsevier Science B.V. All rights reserved.
doi:10.1016/S1570-0232(03)00094-1

requires the further development of suitable pellicular particles for preparative protein chromatography that meet this requirement.
© 2002 Elsevier Science B.V. All rights reserved.

Keywords: Confocal laser scanning microscopy; Adsorption isotherms; Pore diffusion; Mass transfer; Adsorbents; Preparative chromatography; Proteins

1. Introduction

In preparative protein chromatographical processes a high throughput is desired. Contrary to analytical chromatography the process conditions are not limited to the linear part of the adsorption isotherm. The throughput is determined by the rate of mass transfer in and out of the porous particles, the maximum binding capacity and the dissociation constants for the interactions between the protein and the binding sites in the adsorbent particles. In a phenomenological sense this throughput is similar to the space time yield in enzyme technological processes using enzymes immobilized in porous particles [1]. The mass transfer problems in both cases are similar. To study the factors that limit the mass transfer rate in the porous particles used in chromatography and enzyme technology requires the direct determination of the concentration of free and adsorbed molecules, substrates and products as a function of time in- and outside single particles. For particles with immobilized enzymes this has been done using microfluorometry and microelectrodes [2,3]. These results showed that large substrate concentration gradients can be formed in the diffusion layer (film) outside the particles. The dynamic pH gradients formed in these particles during hydrolysis reactions have been measured by confocal laser scanning microscopy (CLSM) [4].

Protein diffusion in particles for size-exclusion chromatography has been studied by microinterferometry and microfluorometry [2,5]. With these methods the concentration gradient along a diameter is not observed directly, but can be calculated from the interference patterns. CLSM has recently been used to determine the concentration of adsorbed molecules along a diameter as a function of time in particles for adsorption chromatography with a resolution in the μm range. The particles had been washed after adsorption of fluorescent molecules for different times [6–10]. Therefore not the same particle was measured at the different adsorptions times. These measurements allow only indirect conclusions on the rate of mass transfer in the particles, as the free molecules are not measured. In these measurements a slight maximum (hump) in the concentration of adsorbed molecules inside the particles, approximately 0.8–0.9 R from the particle center, was consistently observed for both biospecific and ion-exchange adsorbents. For the latter adsorbents it has been explained as an effect caused by the electrical double layer on the surface of these adsorbents [11]. In all the microscopic and CSLM studies the final concentration at the border of the particles did not show a vertical increase expected for particles with a constant solid-phase content along a radius. The concentration of the adsorbed molecules was found to increase for distances 10–30% of the radius from the outer particle surface for both macroporous and polymeric network adsorbents with radii in the range of 20–100 μm (Fig. 1) [5–10]. The larger % value applies for the smaller

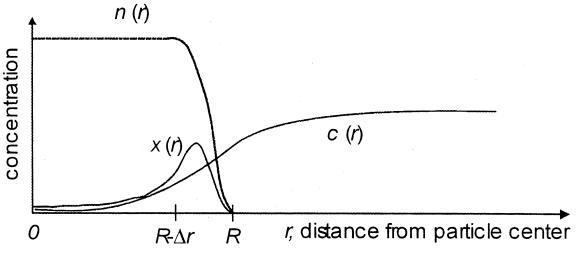

Fig. 1. The concentration of free $c(r)$ and adsorbed $x(r)$ molecules in and outside an adsorbent particle with radius R at the start of an adsorption process. The maxima in $q(r)=c(r)+x(r)$ have been observed in [5–9]. The adsorbent particle has a decreasing solid-phase and binding site content $n(r)$ in the spherical shell between $R-\Delta r$ and R, as has been observed in Ref. [4]. The concentration of free molecules outside the particle is determined by the film theory, inside the particle equilibrium between bound and free molecules is assumed.

particles. The maxima (humps) observed in the concentration of adsorbed molecules just inside the particle may be also be caused by a gradient in solid-phase content and a higher content of macropores or void space in this particle region [5]. This also follows from the 'roughness' of the particle surface observed by microscopy [12]. This results in a decrease in the binding site concentration in the outer part of the adsorbent particle.

The aim of this study was to investigate whether this solid-phase gradient causes the maxima, to determine the rate-limiting step in the equilibration of the adsorption, and whether the kinetics of this process can be described by a linear driving force model [13]. For this purpose the concentration of free and adsorbed molecules in and outside a chromatographic adsorbent particle was determined as a function of time with CLSM. To analyze these data the maximum static adsorption capacity n and the dissociation constant K for the interaction of the adsorbate and the binding sites in the adsorbent particle must be known. They can be determined from Scatchard plots derived from the equilibrium adsorption data [14].

It has been observed that for a biospecific adsorbent for α-chymotrypsin the Scatchard plots were linear at $n<10^{-4}$ M, but become increasingly non-linear with larger n [15]. This indicates that binding sites are shielded by adjacent ligands or already adsorbed molecules when n increases [16]. This leads to a non-ideality condition causing a concentration dependence in the binding constant K. As high n-values are desirable in preparative chromatography, and n and K are important parameters in the design of chromatographic separations, the consequences of such shielding of binding sites were also analyzed.

2. Mass transfer in- and outside chromatographic adsorbents

The mass transfer relations within and outside an adsorbent particle are derived from concentration profiles as shown in Fig. 1. Generally it is assumed that within the particle free, $c(r,t)$, and adsorbed molecules, $x(r,t)$, are in equilibrium. For a Langmuir adsorption isotherm they are related by the equation

$$x(r,t) = n(r)\, c(r,t)/[K + c(r,t)] \tag{1}$$

where $n(r)$ and K are the maximum binding capacity and the equilibrium constant, respectively. Due to the gradient in solid-phase content, $n(r)$ is not constant in the outer part of the particle as shown in Fig. 1. Within the particle the following mass conservation relation applies for a homogeneous pore diffusion model [17,18].

$$\begin{aligned}\epsilon_p \frac{\partial q(r,t)}{\partial t} &= \epsilon_p \cdot \left[\frac{\partial c(r,t)}{\partial t} + \frac{\partial x(r,t)}{\partial t} \right] \\ &= \epsilon_p \left(1 + \frac{\partial x}{\partial c}\right) \cdot \frac{\partial c(r,t)}{\partial t} = D_p \\ &\cdot \left[\frac{\partial^2 c(r,t)}{\partial r^2} + \frac{2}{r} \cdot \frac{\partial c(r,t)}{\partial r} \right]\end{aligned} \tag{2}$$

where D_p is the pore diffusion coefficient, and ϵ_p the particle porosity. As the association reaction to the binding sites occurs in the pore volume of the particles, the concentration of the adsorbed molecules in this volume is used in Eq. (2). Strictly it can only occur in a part of this volume, i.e. in a volume element of the pores outside the surface of the solid-phase. As this part is unknown, the concentration of adsorbed molecules is considered to be homogeneously distributed in the pore volume. In other derivations this concentration applies for the solid volume element $(1 - \epsilon_p)$ where no association reaction can take place [17,18]. Eq. (2) can be rewritten as

$$\frac{\partial c(r,t)}{\partial t} = D_{p,eff} \cdot \left[\frac{\partial^2 c(r,t)}{\partial r^2} + \frac{2}{r} \cdot \frac{\partial c(r,t)}{\partial r} \right] \tag{3}$$

where the effective diffusion coefficient $D_{p,eff}$

$$\begin{aligned}D_{p,eff} &= D_p/[\epsilon_p(1 + dx/dc)] \\ &= D_p/[\epsilon_p\{1 + n(r)K/[K + c(r)]^2\}]\end{aligned} \tag{4}$$

is concentration dependent, i.e. increases with c in the non-linear part of the adsorption isotherm. In the linear part of the adsorption isotherm

$$D_{p,eff} = D_p/\{\epsilon_p\,[1 + n(r)/K]\} \tag{5}$$

is independent on the concentration. A similar expression has been derived in Ref. [18]. When $n(r)$ increases in the outer part of the particle as shown in Fig. 1, $D_{p,eff}$ will decrease in the spherical shell from R to $R - \Delta r$.

3. Material and methods

3.1. Materials

α-Chymotrypsin (CT, EC 3.4.21.1) and penicillin amidase (PA, EC 3.5.1.11,) were obtained from Sigma (Deisenhofen, Germany), purified by affinity chromatography [19,20], and labeled with fluorescein isothiocyanate (FITC, Molecular Probes, Eugene, OR, USA) as described in Ref. [21]. Soybean trypsin inhibitor (STI, Sigma) and monoclonal antibodies (mAbs) against PA were immobilized in CNBr-activated Sepharose (Amerham-Pharmacia, Freiburg, Germany) as described in Refs. [19,20]. CNBr-activated Sepharose and Eupergit C (Röhm, Darmstadt, Germany) were deactivated by incubation in a phosphate buffer of pH 8.0 (ionic strength $I=0.2$ *M*) with 1 *M* ethanolamine at room temperature for 2 h. Eupergit C, PcA-Eupergit C (PA immobilized in Eupergit C), and phenyl-butylamine immobilized in Eupergit C (PBA-Eupergit [22]) were kindly provided by Mr. Boller (Röhm, Darmstadt, Germany). A clarified and concentrated homogenate from a wild-type *E. coli* strain producing PA (ATCC 11105) with 30 000 U/l, was used to study the adsorption of PA from a homogenate to PBA-Eupergit C [20,22]. Fluorescein was obtained from Sigma. All other chemicals were of analytical grade.

3.2. Equilibrium batch adsorption

Known amounts of the molecules to be adsorbed were incubated for 24 h with 50 μl adsorbent (settled volume) in a total volume of 1 ml at pH 8.0 and 25 °C. The concentration of free molecules *c* was then determined by enzyme activity measurements in the supernatant after filtration [19,20]. The concentration of adsorbed molecules *x* was then determined from the mass balance. *K* and *n* were determined from a Scatchard plot, where the concentrations *c* and *x* were considered to be homogeneously distributed over the pore volume of the particle.

3.3. Confocal measurements

Particles were fixed between a microscope slide and a coverslide, mounted as a wedge, by soaking a phosphate buffer of pH 8.0 ($I=0.2$ *M*) with particles into the volume element between the slides (Fig. 2). That they were fixed was checked microscopically by soaking buffer through this volume element. The particle to be observed was selected so that the distance to the nearest neighbour was at least 10 particle diameters. The solution with the molecules to be adsorbed was soaked through the volume element. Then the fluorescence intensity along the diameter parallel to the flow and the microscope slide was measured as function of time (Fig. 2). The dead time between the addition of the fluorochrome solution and the first measurement, taken as time zero, was = 5 s. Fresh solution was soaked through the volume element every 10th s during the first 2 min of incubation, then this was done every 100th s to avoid depletion of molecules around the particles due to adsorption. The samples were exposed to excitation light only during the measurements for 3 s to minimize photo-bleaching.

The measurements of the profiles were performed with a confocal DM IRBE microscope with aquisi-

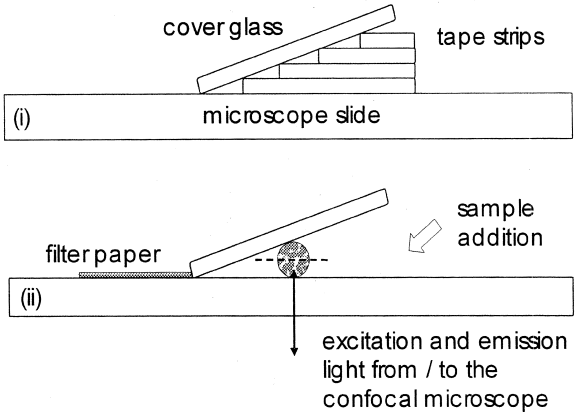

Fig. 2. 'Immobilization' of porous particles for confocal microscopy measurements. (A) Wedge with a distance between the cover glass and the microscope slide of 10–300 μm was formed by glueing tape strips on both sides of the slide. No liquid flow was observed through the tape strips (that can be additionally sealed from the outside by nail laquer). (B) A dilute solution with particles was added and soaked through the wedge until the particles were 'fixed'. Then sample with adsorbate was added to a particle fixed under the cover glass by soaking with a filter paper. The fluorescence intensity was measured along the particle diameter through its center parallel to the direction of the sample flow and the surface of the microscope slide.

tion and evaluation software TCS NT from Leica (Heidelberg, Germany). The magnification was achieved by a 10×0.3 NA dry PL Fluotar lens. An argon/krypton laser with a filter was used to excite the fluorescent molecules at 488 nm. The fluorescence emission was measured using a filter with a maximum at 525 nm. In this work the particles were observed by a horizontal scanning in the optical xy mode within a field of 1000×1000 μm^2, respectively, 512×512 pixels. To reduce noise three scans per image were accumulated. Concentration profiles were determined with the integrated Leica software and modified with Microsoft Excel.

4. Results and discussion

4.1. Equilibrium batch adsorption

For all the systems studied here, Langmuir-type adsorption isotherms were observed. When the experimentally determined concentration of free and bound molecules were plotted as Scatchard plots, non-linear plots were observed for the binding of the proteins to the supports with the highest binding capacity (Fig. 3). For STI-Sepharose the maximum binding site capacity *n*, was as observed previously [15], equal to the amount of immobilized STI within

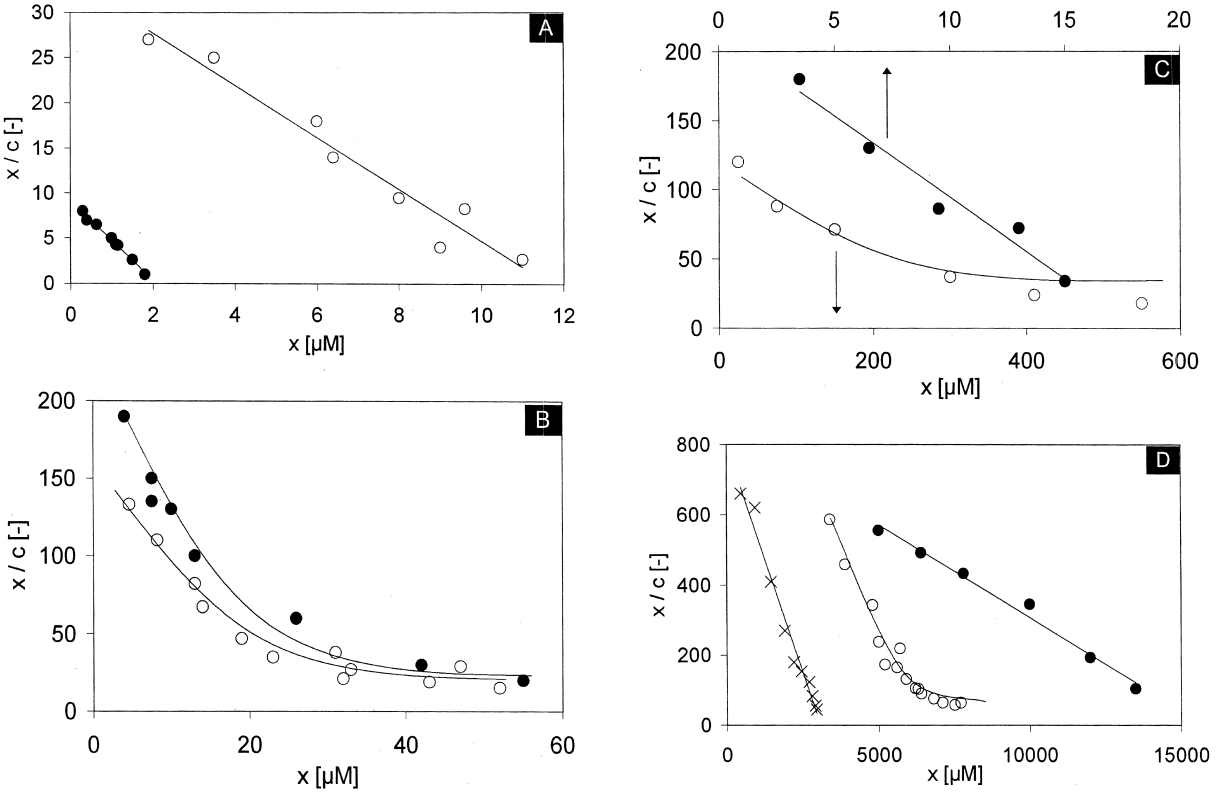

Fig. 3. Scatchard plots for the binding of proteins to biospecific (A, B), hydrophobic and ion-exchange (C, D) adsorbents with different binding capacity and specific surface area. (A) (○) Binding of FITC-PA to mAb-Sepharose (specific surface area ≈10 m^2/ml) at pH 8.0 (I=0.2 M) (this study), (●) binding of CT to STI-Sepharose at pH 7.0 (I=0.2 M) [15]; (B) binding of FITC-CT to STI-Sepharose at: (○) pH 8.0 (I=0.2 M) (this study), (●) pH 7.0 (I=0.25 M) [15]; (C) binding of PA to PBA-Eupergit C (specific surface area ≈40 m^2/ml) in buffer of pH 7.5 (I=0.05 M) with 1 M NaCl from (●) a homogenate with 30 000 U/l or (○) pure PA; (D) (×) binding of bovine serum albumin to 40 μm PEI anion-exchanger (specific surface area 270 m^2/g) at pH 7.5 (3 g salt/l) [18], (●) binding of lysozyme to S-HyperD-M (specific surface area >40 m^2/ml) and (○) Poros 50 HS (specific surface area 25 m^2/ml) at pH 6.5 with 100 and 200 mM NaCl, respectively [17]. All binding experiments were performed at room temperature or 25 °C.

the experimental error. The observed dissociation constant was always larger than for the interaction of the free molecules, indicating that K in this case is perturbed by the immobilization. For the binding of FITC-PA to mAb-Sepharose a linear Scatchard plot was observed (Fig. 3A). In this case the change in K due to the immobilization of mAb has not yet been studied. The wavelength for the maximum fluorescence emission of mAb was changed from 336 to 352 nm upon immobilization [20]. This is due to structural changes that may perturb K for the interaction with free PA.

Non-linear Scatchard plots for the binding of different proteins have been observed previously for biospecific, ion-exchange and hydrophobic adsorbents based on Sepharose, Poros, and porous silica particles when the maximum static capacity n was larger than 0.1 mM [15,23–26]. In the case where only adsorption isotherms were given, Scatchard plots were calculated from these data. Some of them are given in Fig. 3. In Fig. 3C the adsorption of pure PA and PA in a homogenate to PBA-Eupergit C is compared. The adsorption was carried out in the presence of 1 M NaCl to reduce the binding of nucleic acids to this bifunctional adsorbent [22]. It follows that the maximum binding capacity and K is reduced by more than an order of magnitude when PA is adsorbed from a homogenate. For particles with larger specific surface areas, non-linear Scatchard plots were observed first for larger values of n. In the adsorption of low molecular mass molecules as Cephalosporin C to adsorbents with specific surface area of the order of 700 m^2/g, non-linear Scatchard plots have been observed for $n \geq 0.5$ M, at lower concentrations a linear plot was observed [27,28]. The change from linear to non-linear Scatchard plots for CT bound to STI-Sepharose indicates that already adsorbed molecules or neighbouring ligands can shield unoccupied binding sites at high n-values, leading to increasing apparent association constants with increasing n and density of adsorbed molecules [15]. To illustrate this, the average distance between bound molecules at the maximum binding capacity n has been calculated as a function of the specific surface area for different values of n (Fig. 4). From these data follows that for Sepharose with a specific surface area of ≈ 10 m^2/ml support, the distance between the surfaces of adjacent binding

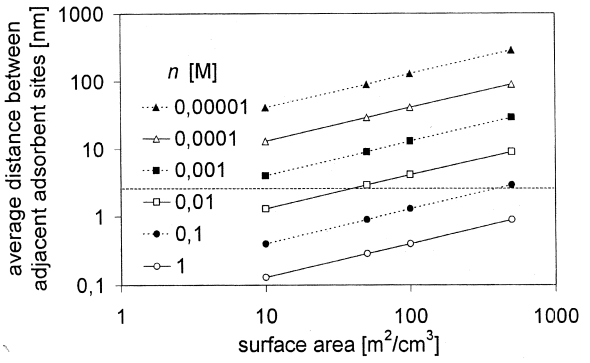

Fig. 4. The average distance of adjacent binding sites on the surface of the pores of chromatographic adsorbents, as function of the specific surface area. They are given for different maximum static binding capacities n. The horizontal dotted line gives the lower limit for the diameter of proteins ($\approx$2.5 nm).

sites or adsorbed molecules at saturation is about the molecular diameter of proteins when $n \geq 0.1$ mM. For low molecular mass molecules this occurs first at much higher values of n. These results indicate that the analytical description of the adsorption to high capacity adsorbents that are suitable for preparative chromatography must consider this non-ideality that results in non-linear Scatchard plots. The change in the dissociation constant can be due to changes in both the association or dissociation rate constant. For lysozyme immobilized on surfaces it has been shown that the association rate for the binding of five different monoclonal anti-lysozyme antibodies decreases by a factor of 5, compared with the value in free solution [29]. In this case the space angle from which a free protein can collide with the immobilized protein is reduced by at least a factor of two compared to the interaction in free solution. This leads to a reduced collision frequence and association rate constant. This and the shielding of binding sites by adjacent binding sites or already adsorbed molecules leads to a concentration dependence of the apparent binding constant K, compared with the free solution value. These and the adsorption isotherms must then be described by a concentration dependent apparent dissociation constant K. For the non-linear Scatchard plots the apparent K-values were estimated for small ($K_{app,1}$) and saturating ($K_{app,2}$) x values using the relation

$$K_{app,i} = (n - x_i)/(x/c)_i. \quad (6)$$

Table 1
Maximum concentration of binding sites, n, the dissociation constant K, for linear Scatchard plots, and the apparent dissociation constants ($K_{app,1}$) and ($K_{app,2}$) for non-linear Scatchard plots for the adsorption of different molecules in porous particles for chromatography and enzyme technology; the free and adsorbed concentration were determined at 25 °C and pH 8.0 (phosphate buffer with $I = 0.2$ M)

System	n (μM)	K (μM)	$K_{app,1}$ (μM)	$K_{app,2}$ (μM)
Adsorption of fluorescein to inactivated Eupergit C	2000	1000		
Adsorption of FITC-CT to PBA-Eupergit C	1400		10	20
Adsorption of FITC-PA to PBA-Eupergit C	300	3		
Adsorption of FITC-CT to STI-Sepharose	600		3.5	12
Adsorption of FITC-CT to STI-Sepharose	70		0.5	1.4
Adsorption of CT to STI-Sepharose [15]	75		0.5	1.5
Adsorption of CT to STI-Sepharose [15]	8	0.2		
Adsorption of FITC-PA to mAb-Sepharose	18	0.3		

The values of n and K determined for the different systems are given in Table 1. The concentration n is an apparent value as it is the average value over the whole pore volume of the particle. The binding sites are, however, only located in a part of this volume that is difficult to estimate. The results show that for the non-linear plots the determined K_{app}-values increases with n in the range predicted by Fig. 4. They also confirm previous observations that the procedure used to label CT with the fluorochrome influences its adsorption behaviour marginally [21].

Non-linear Scatchard plots are also expected for bi-Langmuir adsorption isotherms. They are observed when there are two classes of binding sites with different dissociation constants. The above results indicate that this does not occur when n is small. When n and x increases adjacent binding sites or already bound molecules cause the observed increase in K for the remaining free binding sites.

4.2. Concentration profiles of free and adsorbed molecules in and outside the particles as function of time

By measuring the intensity of fluorescein solutions the fluorescence intensity was found to be linear in the concentration range 1–500 μM. Thus outside the particles the concentration can be directly proportional to the observed intensities in this concentration range.

In the observed intensity profiles after different times of adsorption the bulk concentration outside the film was constant. It equals the concentration of the used fluorochrome solution. The intensity profiles were then converted to concentration curves. The concentration inside the particles is then an apparent value q_{app} (see below). Such curves for different adsorption times are shown in Figs. 5 and 6 for the adsorbents: inactivated Eupergit C, PcA-Eupergit C, PBA-Eupergit C, STI-Sepharose, mAb-Sepharose and inactivated Sepharose. They show the same shape, with a maximum in the intensity of adsorbed and free molecules, whose distance from the outer particle surface increases with time. Finally distances of $\Delta \approx 6$–8 μm for the particles with $R > 50$ μm and up to $\Delta r \approx 20$ μm for an Eupergit particle with $R = 50$ μm are reached. This is of the same magnitude as observed previously for washed particles [6–10]. This supports the assumption that the observed maxima are due to a decrease in solid-phase content and n between $(R - \Delta r)$ and R. Then $x(r,t)$ will first increase inside the particles, as $n(r)$ increases. Further inside the particles where n is constant or decreases $x(r,t)$ will decrease. This results in the observed maxima (Fig. 6).

Inside the particles the following three effects must be considered to calculate the total concentration of protein in the pore volume $q(r,t) = x(r,t) + c(r,t)$ from the apparent concentrations in Figs. 5 and 6:

(a) The pore fraction of the observation window of the confocal microscope;

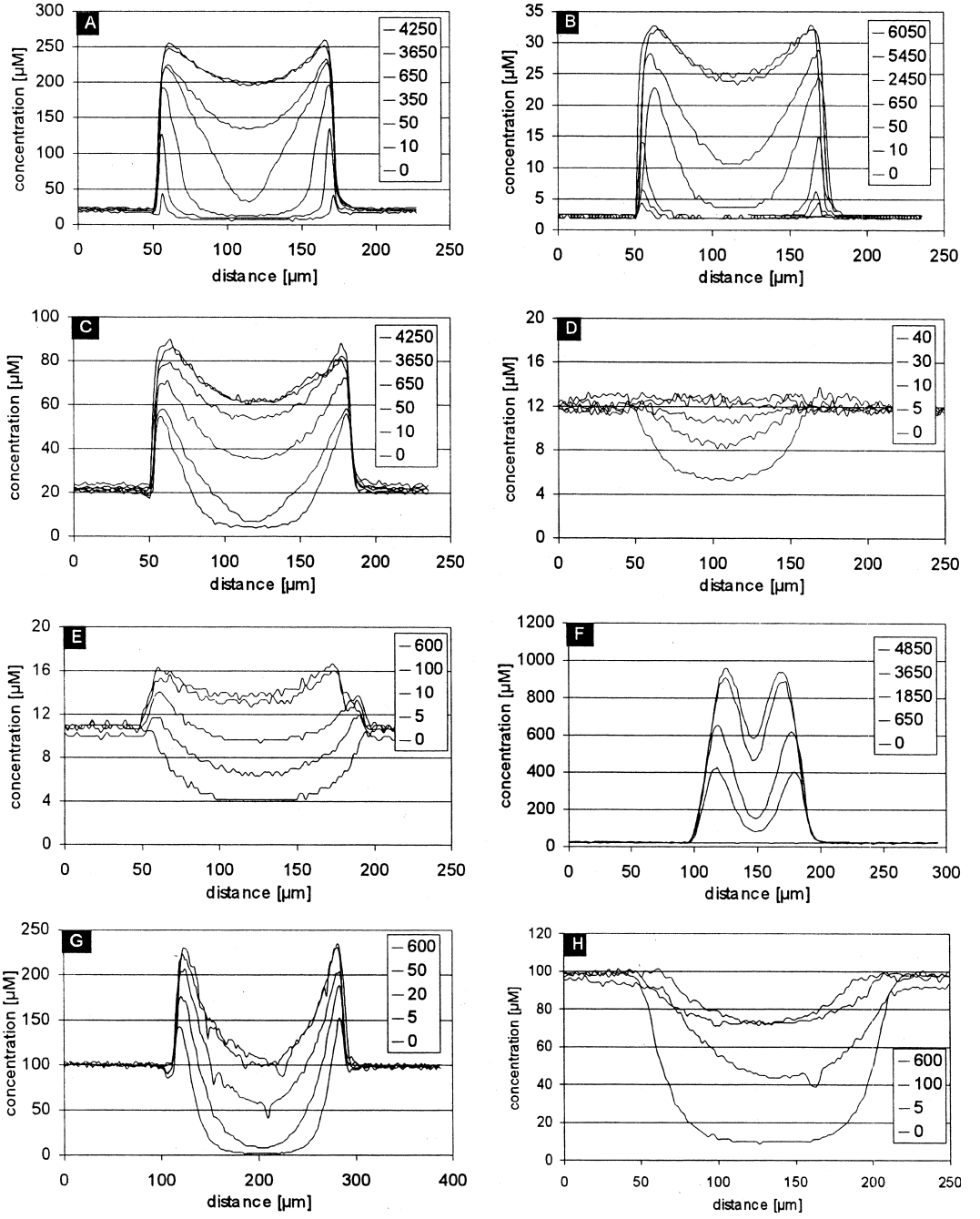

Fig. 5. The concentration of free outside and free and adsorbed molecules inside a single porous particle for adsorption chromatography as function of incubation time (given in seconds in the upper right corner). All experiments were carried out in phosphate buffer of pH 8.0 ($I=0.2$ *M*) and 25 °C. The concentration inside the particles is an apparent concentration (see text). (A) Adsorption of 22 μ*M* FITC-CT to STI-Sepharose ($n=600$ μ*M*); (B) adsorption of 2.2 μ*M* FITC-CT to STI-Sepharose ($n=600$ μ*M*); (C) adsorption of 22 μ*M* FITC-CT to STI-Sepharose ($n=70$ μ*M*); (D) adsorption of 12 μ*M* FITC-CT to Sepharose without binding sites; (E) adsorption of 11 μ*M* FITC-PA to STI-Sepharose ($n=600$ μ*M*); (F) adsorption of 22 μ*M* FITC-CT to PBA-Eupergit C ($n=1400$ μ*M*); (G) adsorption of 100 μ*M* Fluorescein to inactivated Eupergit C; (H) adsorption of 100 μ*M* Fluorescein to PcA-Eupergit C.

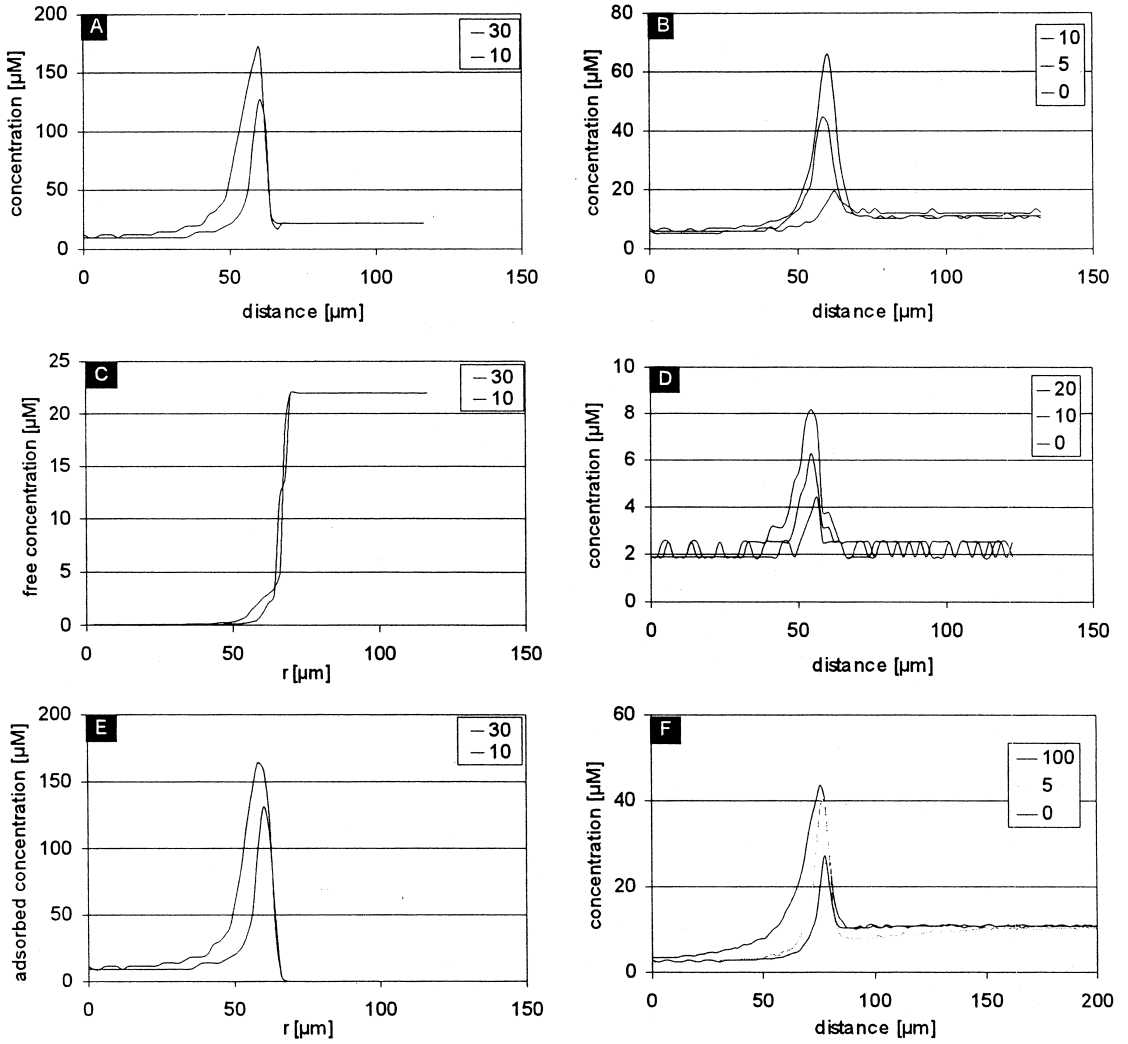

Fig. 6. The concentration profiles along a particle radius and outside the particles at the start of adsorption experiments as shown in Fig. 6. The times after the start of the adsorption are given in seconds in the upper right corner. In (A), (B), (D) and (F) the inside concentrations are the apparent concentrations q_{app} (Eq. (7)). (A) Adsorption of 22 μ*M* FITC-CT to STI-Sepharose ($n=600$ μ*M*); (B) adsorption of 12 μ*M* FITC-CT to STI-Sepharose ($n=600$ μ*M*); (C) calculated values for the free FITC-CT in (A); (D) adsorption of 2.2 μ*M* FITC-CT to STI-Sepharose ($n=600$ μ*M*); (E) calculated values of adsorbed FITC-CT (x) in (A); (F) adsorption of 11 μ*M* FITC-PA to PBA-Eupergit C ($n=1400$ μ*M*).

(b) Internal reflections within the support that reduces the fluorescence intensity of the observed fluorochromes and
(c) Changes in the fluorescence intensity when a fluorochrome is adsorbed to a binding site.

(i) The linear dimensions of the confocal observation volume (≈0.5 μm) is larger than the pore size of the studied particles. Then the fluorescence intensity within the particles is the sum of the intensities of the average free (c) and adsorbed (x) molecules multiplied by the pore volume fraction ϵ_p of the particles.
(ii) When FITC-CT was added to Sepharose the final intensity inside the particles was found to

be constant over the particle and almost equal to the intensity outside the particle (Fig. 5D). The slight increase observed might be due to a weak adsorption of positively charged FITC-CT to negatively charged groups on Sepharose. In this case intensity changes due to internal reflections within the particle can be neglected. This was not observed for PcA-Eupergit that does not adsorb fluorescein (Fig. 5H). The intensity decreased to a minimum in the middle of the particle due to internal reflections in this macroporous support.

(iii) The labeling procedure of the proteins used here gives mainly mono-labeled proteins where the fluorescein is covalently bound to different lysines on the protein surface [21,30]. For FITC-CT and FITC-PA the dissociation constants for the interaction with immobilized STI or mAb were found to be practically the same as for the unlabeled proteins. In the complex with STI the fluorescence intensity of mono-labeled FITC-CT is 30% lower than for free FITC-CT [19]. For FITC-PA no change in fluorescence intensity was observed when it was bound to the mAb [30]. When FITC-PA or FITC-CT are adsorbed to PBA-Eupergit it was assumed that the change in fluorescence intensity was negligible. This was based on the observation that the fluorescense intensity of the labeled proteins changed by less than 5% in the presence of 5 m*M* phenylacetic acid, a known competitive inhibitor of these enzymes with $K_i \approx 0.01$ m*M* [31].

From (a)–(c) it follows that the concentration of free and adsorbed molecules inside the particles can be calculated from the apparent concentration for STI- and mAb-Sepharose in Figs. 5 and 6 as follows. Equilibrium between adsorbed and free molecules, and a concentration independent K (linear Scatchard plot) were assumed. Then the apparent concentration at any point and at time t within the particle is

$$q_{app}(r,t) = [\epsilon_p\{\alpha\, x(r,t) + c(r,t)\}] = \epsilon_p\,[\alpha\, n(r)\, c(r,t)/\{K + c(r,t)\} + \epsilon_p c(r,t)] \quad (7)$$

where α is the ratio of the fluorescence intensity of an adsorbed to a free fluorochrome-labeled protein. When $x(r,t) \gg c(r,t)$

$$q(r,t) = q_{app}(r,t)/(\epsilon_p\, \alpha) \quad (8)$$

For other cases $c(r,t)$ can be calculated from the following relation derived from Eq. (7)

$$c^2[r,t) + (\alpha\, n(r) + K - q_{app}(r,t)/\epsilon_p)\, c(r,t) - q_{app}\,(r,t)\, K/\epsilon_p = 0 \quad (9)$$

From the final values of $q_{app}(r)$, where adsorption equilibrium has been reached, $n(r)$ can be calculated from Eq. (6). This gives

$$n(r) = [\{q_{app}(r)/\epsilon_p - c_b\}(K + c_b)]/\alpha c_b \quad (10)$$

In case that the Scatchard plot is non-linear, K_{app} values must be estimated for the x-values involved in the experiment. To calculate $c(r,t)$ and $x(r,t)$ for the initial adsorption in STI-Sepharose (Fig. 6A) in the spherical shell between R and $(R-2\ \Delta r)$ Eqs. (7)–(10) were used. Eq. (8) applies for this case, and $K_{app,1}$ and $K_{app,2}$ (Table 1) were used in Eqs. (9) and (10), respectively. The other constants used here are $\alpha = 0.7$ and $\epsilon_p = 0.95$. The calculated values of $c(r,t)$ and $x(r,t)$ are given in Fig. 6C and E. The results show that at the start of the adsorption there is a steep concentration change in the free molecules just inside the outer particle surface, and a maximum in $x(r,t)$ in agreement with the observed experimental data. The values of x in Fig. 6E are larger than the q_{app}-values in Fig. 6A, as the latter are uncorrected concentration values (Eq. (8)).

Within the Sepharose particles $n(r)$ was not found to be constant within $(R - \Delta r)$ for the particles studied here (Fig. 5A–F). When the average n value determined from the adsorption isotherms increased from 70 to 600 μ*M*, the minimum value observed in the middle of the particle increased from 60 to 80% of the maximum value. The immobilization conditions used were selected to immobilize more than 90% of the free protein, i.e. then the support is not saturated with immobilized protein. With excess protein and reduced immobilization yield n, will become constant within $(R - \Delta r)$, as was observed in Ref. [10]. The difference observed here does only influence the adsorption capacity of the particle marginally, as only 10% of the capacity is due to adsorption within $R/2$ from the particle center.

4.3. Rate limiting step in the adsorption

This can be analyzed from the experimental data shown in Figs. 5 and 6. For most of the systems studied here more than 90% of the bulk concentration is reached just outside the adsorbent particles within 5 s. For these this concentration was practically constant during the adsorption process. In some cases, especially for PBA-Eupergit with a high binding site concentration, a larger concentration gradient in the film is observed, where the concentration just outside the particles is about 70% of the bulk content 20 s after the start of the adsorption (Fig. 6F). The thickness of the unstirred diffusion layer determined from the slope of this gradient is approximately equal to the particle radius. This is expected for an unstirred system where the Sherwood number is 2 [3]. This shows that the occasional addition of stock solution to maintain a constant bulk content did hardly change the Sherwood number from 2. After 50 s the concentration change in the film was less than 10% of the bulk concentration. These results show that intraparticle mass transfer is the rate limiting step of adsorption in the different systems studied here, covering a large range of n/K or x/c values, low and high molecular mass substances and bulk concentrations from $<K_{app}$ to $>10K$ or K_{app}.

The adsorption profiles in single particles (Fig. 5) can also be used to estimate the minimum residence time of a sample in a chromatographic column with the same particles required to utilize >90% of the static column capacity. This is frequently determined from breakthrough curves. When the same conditions as above apply for the column these times are of the order of 1000 s for the particle sizes and conditions used in Fig. 5A and C. These times are about the same as have been determined from breakthrough curves under similar conditions [32]. When the column length L is given, these times can be used to calculate the linear flow-rates u required to obtain the required residence time.

4.4. Rate of adsorption and its driving force; evidence for a two-step linear driving force model

The results in Fig. 5 show that the times to reach the adsorption maximum are much smaller in the outer than in the inner part of the particles. This was observed also for the adsorbents not shown in this figure. All experiments were carried out in the non-linear part of the adsorption isotherm. The times required to reach the adsorption maximum were found to decrease when the bulk concentration was increased. This is in agreement with Eq. (4), where it was shown that $D_{p,eff}$ increases with the concentration in the non-linear part of the adsorption isotherm. These results show that the adsorption process can be described as a sum of a rapid and a slow process. Such two-step adsorption kinetics has been observed for both low-molecular mass compounds [27,28,33], proteins [17,18,23,25,34–36] in batch adsorption experiments using different adsorbent particles.

From the concentration profiles in Fig. 5 the average value of the concentration of free and adsorbed molecules $\langle q(t)\rangle$ in the particle can be calculated as a function of time using Eqs. (7)–(10). This was done for the equilibration of CT and STI-Sepharose, where the fluorescence intensity is linear in concentration, and the decrease in the fluorescence due to internal reflections (observed in the Eupergit particles) can be neglected (Fig. 5D). When the final value did not change in the last 1000 s, it was considered that equilibrium adsorption has been obtained. The final average concentration is q^*. When equilibrium had not been obtained this value was determined from the equilibrium adsorption isotherm. The plot of $\log [1-\langle q(t)\rangle/q^*]$ in Fig. 7 shows that the equilibration to more than 90% of the final value can be described by a two-step linear driving force model. Then the following relation applies

$$\log\left[1-\frac{\{\langle q_1(t)\rangle+\langle q_2(t)\rangle\}}{(q_1^*+q_2^*)}\right] = \log\left(\frac{q_1^*}{q^*}\cdot e^{-k_{ads,1}t}+\frac{q_2^*}{q^*}\cdot e^{-k_{ads,2}t}\right) \quad (11)$$

where $q^*=(q^*_1+q^*_2)$, and the subscripts 1 and 2 denote the binding sites that equilibrate rapidly and slowly, respectively. The rate constants $k_{ads,1}$ and $k_{ads,2}$ were determined from the slopes of the linear parts of the graphs in Fig. 7. They and some values calculated from published batch equilibration curves are given in Table 2. In the latter case $k_{ads,1}$ and $k_{ads,2}$

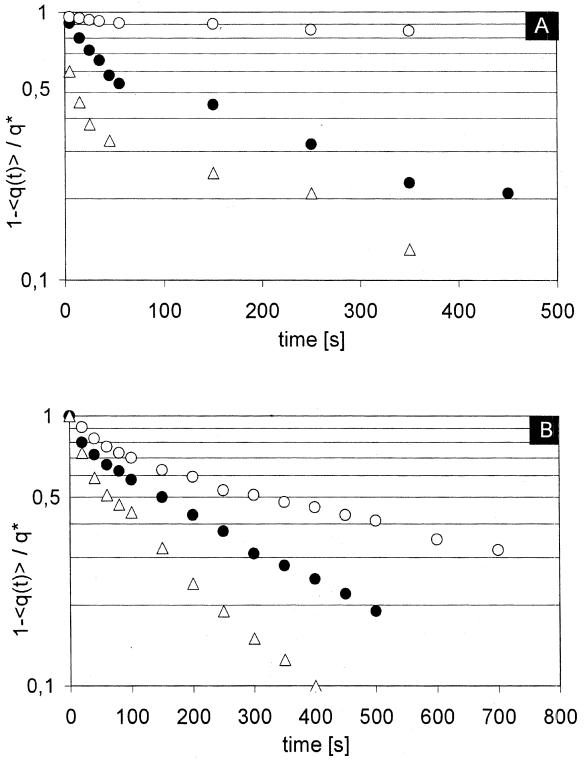

Fig. 7. Log$(1-\langle q(t)\rangle/q^*)$ as a function of time for the adsorption of proteins in single particles at constant bulk (c_b) concentrations (A) or from batch adsorption experiments, where the bulk concentration decreases with time (B). (A) ○ Adsorption of 2.2 μ*M* FITC-CT to STI-Sepharose ($n=600$ μ*M*); ● adsorption of 22 μ*M* FITC-CT to STI-Sepharose ($n=600$ μ*M*); △ adsorption of 22 μ*M* FITC-CT to STI-Sepharose ($n=70$ μ*M*) (conditions as in Fig. 5). (B) Adsorption of lysozyme at different initial bulk concentrations (○ 35 μ*M*, ● 70 μ*M*, △140 μ*M*) to the same amount of POROS 50 HS ($n=12000$ μ*M*) in 10 m*M* phosphate buffer of pH 6.5 at room temperature [15].

were only determined when the change in the bulk concentration was small during the batch adsorption. When this was not the case only $k_{ads,1}$ was determined.

As expected from Eq. (4) $k_{app,1}$ decreases with n, and increases with c_b. The adsorption was always carried out in the non-linear part of the adsorption isotherm, and $D_{p,eff}$ is expected to increase by a factor of >10 for $n>50$ μ*M*, when c_b increases from K_{app} to 10 K_{app}. The results show that $k_{ads,1}$ applies for 30 to 50% of the maximum adsorption capacity. This is as shown in Fig. 5 mainly located in the outer part of the particle between $r=R$ and $r\approx(R-2\,\Delta r)$. The slower adsorption occurs between $(R-2\,\Delta r)$ and $r=0.4\,R$ and accounts for 40 to 60% of amount adsorbed. The linear driving force rate constants can be related to the half life time for diffusion that is proportional to $(R^2/D_{p,eff})$. Based on this the following expression for k_{ads} for a one-step adsorption process that can be described by a linear driving force has been derived [37,38].

$$k_{ads} = 15(D_{p,eff}/R^2) \tag{12}$$

where the constant 15 was derived from the assumption that the concentration profile in the particle can be expressed by a quadratic expression in q. This is as follows from Fig. 5 not justified. The results obtained here show that the mean diffusion distance to the part of the particle that has reached adsorption equilibrium should be used in Eq. (12) instead of the particle radius. They are ≈0.1 R and 0.3 R for the rapid a slow process, respectively. More than 90% of the binding sites are located outside the radius 0.4 R. From R to $(R-\Delta r)$, $D_{p,eff}$ decreases from D_p to $D_p/(\epsilon_p\ [1+nK/\{K+c(r)\}^2])$ that is the value that applies for the inner region of the particle (Eq. (4)). This decrease in $D_{p,eff}$ and the increasing diffusion distance causes the slower rate of equilibration in the inner part of the particles. (Table 2).

In some of the batch experiments the rapid initial phase and subsequent slow adsorption rate were explained to be due to transport through the external film and pore diffusion [17,18] or rapid diffusion in macro- and micropores [32], respectively. Whether this applies can be analyzed by the ratio of the maximal adsorption rate in the particle, to the maximal mass transfer rate to the particle. This is a dimensionless number (similar to the Thiele modulus or Damköhler number in heterogeneous catalysis or enzyme technology [1]) first introduced for chromatography in Ref. [39]. For the rapid adsorption process described by Eq. (11) it can be written as

$$\frac{\text{maximum rate of adsorption in outer part of the particle}}{\text{maximum rate of transport through film}} = \frac{\frac{4}{3}\pi(1-\alpha^3)R^3 k_{ads,1} q_1^*}{4\pi R^2 \cdot \frac{D_s Sh}{2R} c_b} = \frac{2}{3}\cdot\frac{(1-\alpha^3)R^2 k_{ads,1}}{D_s Sh}\cdot\frac{q_1^*}{c_b} \tag{13}$$

Table 2
The rate constants $k_{ads,1}$ and $k_{ads,2}$, the fraction of adsorbent sites q_1/q^* and q_2/q^* with these rates for adsorption that can be described by the bilinear kinetic Eq. (12); they are determined for protein adsorption to single particles at constant bulk content c_b, or in batch experiments with a large number of particles, with average radius R, where the bulk content decreases during the experiment. K_{app} and n were determined from Scatchard plots and Eq. (6); (BA = biospecific adsorbent; HA = hydrophobic adsorbent; IEA = ion-exchange adsorbent), for comparison the data are also given for the adsorption of a low molecular mass compound (Cephalosporin C) (≈indicates a large experimental error)

Adsorbent/type	R (μm)	Adsorbate M_r	c_b μM	$k_{ads,1}$ s^{-1}	$k_{ads,2}$ s^{-1}	q_1/q^*	q_2/q^*	n μM	K_{app} μM	Source
STI-Sepharose/BA	60	α-Chymotrypsin	22	0.02	0.0014	0.5	0.4–0.5	600	12	This work
		(25 000)	2.2	0.0017		0.3	0.6–0.07	600	3.5	
STI-Sepharose/BA	60	α-Chymotrypsin	22	≈0.1	0.007	0.		70	1.4	This work
			2.2	0.02	0.0035	0.4	0.6–0.6	70	0.5	
Batch adsorption										
STI-Sepharose/BA	40	α-Chymotrypsin	20	0.015		0.4		300	5	[33]
STI-Eupergit 250 L/BA	80	α-Chymotrypsin	20	0.02		≈0.3		260	10	[34]
Protein A-Eupergit 250 L/BA	80	mAb (150 000)	3	0.005		≈0.3		120	5	[35]
STI-LiChrospher/BA	10	α-Chymotrypsin	20	0.02	–	>0.8		3300	1	[32]
Procion Blue MX-R-silica/BA	6	Lactate dehydrogenase (140 000)	not given	≈0.1				60	0.2	[25]
Polyethyleneamine-silica/IEA	7.5	Bovine serum albumin (67 000)	20	≈0.04	0.002	0.4	0.5–0.6	3000	4	[18]
TosoHaas SP650C/IEA	55	Lysozyme (14 000)	16	≈0.01		0.3		3000	≈10	[23]
POROS 50 HS/IEA	20	Lysozyme	140	0.02	0.007	0.3	0.6–0.7	12 000	≈20	[17]
S-HyperD-M/IEA	40	Lysozyme	140	0.014	0.003	0.5	0.4–0.5	16 000	20	[17]
XAD-16/HA	280	Cephalosporin C (400)	5000	0.004	0.001	≈0.5	≈0.4–0.5	150 000	5000	[28]

where D_s is the diffusion constant in free solution, Sh the Sherwood number (two in the experiments shown in Fig. 5 and ≈10 in column chromatography [36]), and α the fraction of the radius outside which the rapid adsorption process occurs. This ratio is >1 and <1 for a process where the rate limiting step is external or intraparticle mass transfer, respectively. From Eq. (13) follows that external mass transfer limitation can be expected for large R and q^*_1/c_b values. The condition for intraparticle mass transfer as a rate-limiting step for the rapid adsorption step is thus

$$k_{ads,1} < 1.5 \cdot \frac{D_s Sh}{(1-\alpha^3)R^2} \cdot \frac{c_b}{q_1^*} \quad (14)$$

This condition is fulfilled for all the adsorptions into single particles shown in Fig. 5, where the adsorbate concentration was ≈c_b at the particle surface. Except for the most unfavorable batch adsorption case (Cephalosporin adsorption to XAD 16 with large R or q^*_1/c_b) in Table 2 the initial adsorption step fulfills the condition Eq. (14). They are all performed in the non-linear part of the adsorption isotherm. From these results follows that for typically protein adsorbents with $R<100$ μm, external mass transfer limitation can always be avoided when the adsorption is carried at bulk concentrations $>K_{app}$. Then the rate of adsorption also increases with c_b.

As expected the equilibration of a low-molecular mass adsorbate is much faster than for proteins as their diffusion coefficients differ by almost an order of magnitude (Fig. 5F). The results shown here and in Table 2 indicate that the assumption of rapid equilibration between mobile and solid-phase of low-molecular mass molecules in chromatography is not generally justified [40,41].

The desorption was not studied here, but the following qualitative conclusions can be derived from the results for adsorption presented here. Generally the adsorption step in preparative chromatography will not be carried out to equilibrate the whole adsorbent with the bulk protein content. This would require long residence times. At the end of the adsorption only the outer part of the particle will be equilibrated with bulk content as shown in Fig. 5. At

the start of the desorption there will be two protein concentration gradients, one in the outer part and one in the interior of the particle. Then there will be a flow of adsorbed proteins out of the particles and further into the particles. During an isocratic desorption process after an adsorption in the non-linear part of the adsorption isotherm, $D_{p,eff}$ will always be smaller than during the adsorption. Thus the rate of such a desorption process will, under isocratic conditions, be smaller than for the adsorption. Due to the higher concentration of free protein and the larger $D_{p,eff}$ in the outer part of the particles, the protein there will desorb faster than in the inner part of the particles behind the adsorption maximum (Fig. 5). Due to the flow into the particle interior there will be a considerable tailing in the desorbed protein. The concentration of desorbed protein at the particle surface as a function of time will therefore have a steep front and a long tail, i.e. the same shape as a protein peak at the end of a chromatographic column [13,42]. By reducing the diffusion distance to the particle surface, the contribution to this tailing due to protein diffusion from the inner part of the particles, could be reduced. This has been realized for perfusible supports of the same size as the adsorbents studied here [12]. The plate height at superficial velocities that allow convectional flow through the particles, was much smaller than for non-perfusible supports of the same size. For the latter the diffusion distance and the tailing can be reduced as follows with marginal loss in capacity. Within $r = 0.5\ R$ from the particle center $\approx 10\%$ of the adsorption capacity is located. The rate of desorption would be increased and the tailing reduced when no adsorption is possible in this part of the adsorbent particle. Narrower particle size distributions should also be used for this aim.

5. Conclusions and consequences for preparative protein chromatography

In preparative chromatography the adsorbent and n and K_{app} are usually given. The adsorption is generally carried out under isocratic conditions. The problem is to select c_b for a high throughput and protein recovery. The results presented here show that c_b should be selected in the non-linear part of the adsorption isotherm, i.e. $> K_{app}$ where the adsorption rate increases with c_b (Eq. (4) and Table 2). The upper limit is given by the condition that $x/c_b \geq 10$ to obtain a protein recovery of $>90\%$. A higher protein recovery can be obtained by choosing a lower c_b, but this will reduce the adsorption rate and the throughput as $D_{p,eff}$ will decrease (Eq. (4)). Then also more adsorbent is required to adsorb the protein in in a given sample.

The rate of adsorption has been shown here to be controlled by the intraparticle mass transfer, when c_b lies in the non-linear part of the adsorption isotherm. This rate could as shown here, and for many published systems, be described by a bilinear free driving force model, whose rate is proportional to $D_{p,eff}/R^2$. Then the rate constants for the adsorption $k_{ads,1}$ and $k_{ads,2}$ in Eq. (11) can be determined from batch adsorption experiments. From these the residence time required for a desired degree of adsorbent equilibration can be calculated. For the adsorbents studied here, the time required for the second half of 90% equilibration, is an order of magnitude larger than for the first half. This shows that there is an optimal residence time for adsorption to obtain a high throughput. For preparative affinity chromatography of proteins the optimal residence time (flow-rate, or column length), where also the desorption must be considered, can be determined as shown in Refs. [32,43].

The above applies not only for adsorption to adsorbents that specifically adsorb one protein from a clarified medium or homogenate. When the adsorption isotherm for a protein to be isolated is known, it applies also for adsorbents where other proteins, nucleic acids and other molecules compete for the binding sites in the adsorbent. In this case the adsorption isotherm for the desired protein is

$$x = \frac{nc}{K\left(1 + \sum_{i=1} \frac{c_i}{K_i}\right) + c} \tag{15}$$

where i denotes the ith competing protein, nucleic acid or other molecules. When the adsorbents in a column have equilibrated, c and c_i are the concentrations in the medium or homogenate. In these the ratios $c_i/c = \alpha_i$ are constants and Eq. (15) can be rewritten as

$$x = \frac{nc}{K + c\left[1 + K\left(\sum_{i=1} \frac{\alpha_i}{K_i}\right)\right]} \tag{16}$$

From this follows that the maximum static capacity in this case is not n, observed for the pure protein, but

$$\frac{n}{\left[1+K\left(\sum_{i=1}\frac{\alpha_i}{K_i}\right)\right]}=n/a \tag{17}$$

that is smaller than n. This has also been observed in Fig. 3C where the Scatchard plot has been determined for the adsorption of pure PA and PA in a homogenate to the same hydrophobic adsorbent (PBA-Eupergit C). This adsorbent adsorbs practically all proteins in an *E. coli* homogenate [22]. The capacity for PA from this is about 3% of the capacity for pure PA, and is approximately equal to the fraction of PA of all proteins in the homogenate. For this case the effective pore diffusion coefficient (Eq. (4)) will be

$$D_{\mathrm{p,eff}}=\frac{D_{\mathrm{p}}}{\epsilon_{\mathrm{p}}\cdot\left(1+\dfrac{nK}{(K+ca)^2}\right)} \tag{18}$$

or larger than for the pure protein of the same concentration c as $a>1$ (Eq. (17)), i.e. the rates of adsorption of a protein are expected to be larger with homogenates than with pure protein.

Acknowledgements

We thank Dr. Manfred Schmidt, Zoology Department, University of Hamburg, for valuable assistance in the measurements with the confocal microscope.

References

[1] V. Kasche, Enzyme Microb. Technol. 5 (1983) 2.
[2] M. Sernetz, H. Puchinger, C. Couwenbergs, M. Ostwald, Anal. Biochem. 72 (1976) 24.
[3] V. Kasche, G. Kuhlmann, Enzyme Microbiol. Technol. 2 (1980) 309.
[4] A. Spiess, V. Kasche, Biotechnol. Progr. 17 (2001) 294.
[5] M. Sernetz, O. Hannibal-Friedrich, M. Chun, Micr. Acta 81 (1979) 393.
[6] H.B. Kim, M. Hayashi, K. Nakatani, N. Kitamura, K. Sasaki, J. Hotta, H. Masuhara, Anal. Chem. 68 (1996) 409.
[7] A. Ljunglöf, R. Hjorth, J. Chromatogr. A 743 (1996) 75.
[8] A. Ljunglöf, J. Thömmes, J. Chromatogr. A 813 (1998) 387.
[9] M. Ahmed, D.L. Pyle, J. Chem. Technol. Biotechnol. 74 (1999) 193.
[10] A. Ljunglöf, M. Larsson, K.-G. Kuttila, J. Lindgren, J. Chromatogr. A 893 (2000) 235.
[11] A.I. Liapis, B.A. Grimes, K. Lacki, I. Neretniks, J. Chromatogr. A 921 (2001) 135.
[12] D.C. Nash, H.A. Chase, J. Chromatogr. A 807 (1998) 185.
[13] J.C. Bellot, J.S. Condoret, Process Biochem. 26 (1991) 363.
[14] R.E. Shields, W.G. Bardsley, J. Theor. Biol. 63 (1976) 1.
[15] V. Kasche, Stud. Biophys. 35 (1973) 45.
[16] A. Velayudhan, Cs. Horváth, J. Chromatogr. A 663 (1994) 1.
[17] L.E. Weaver, G. Carta, Biotechnol. Progr. 12 (1996) 342.
[18] J.R. Conder, B.O. Hayek, Biochem. Eng. J. 6 (2000) 215.
[19] D. Gabel, H. Amneus, V. Kasche, J. Chromatogr. 120 (1976) 391.
[20] V. Kasche, N. Gottschlich, Å. Lindberg, C. Niebuhr-Redder, J. Schmieding, J. Chromatogr. A 660 (1994) 137.
[21] V. Kasche, I. Büchtmann, Hoppe Seyler's Z. Physiol. Chem. 362 (1981) 1007.
[22] V. Kasche, T. Scholzen, Th. Boller, D.M. Krämer, F. Löffler, J. Chromatogr. 510 (1990) 149.
[23] C. Chang, A.M. Lenhoff, J. Chromatogr. A 827 (1998) 281.
[24] H. Kitano, K. Nakamura, Y. Hirai, T. Kaku, N. Ise, Biotechnol. Bioeng. 31 (1988) 547.
[25] A.G. Livingston, H.A. Chase, J. Chromatogr. 481 (1989) 159.
[26] A.I. Liapis, B. Anspach, M.E. Findley, J. Davies, M.T.W. Hearn, K.K. Unger, Biotechnol. Bioeng. 34 (1989) 467.
[27] M. Hicketier, K. Buchholz, Appl. Microbiol. Biotechol. 32 (1990) 680.
[28] S.A. Yang, D.L. Pyle, J. Chem. Technol. Biotechnol. 74 (1999) 216.
[29] I. Chaiken, S. Rose, R. Carlsson, Anal. Biochem. 201 (1992) 197.
[30] T. Wiesemann, Thesis TU, Hamburg–Harburg, 1993.
[31] D. Warburton, P. Dunnill, M.D. Lilly, Biotechnol. Bioeng. 15 (1973) 13.
[32] S. Katoh, T. Kambayashi, R. Deguchi, F. Yoshida, Biotechnol. Bioeng. 20 (1978) 267.
[33] D.C.S. Azevedo, A.E. Rodrigues, Ind. Eng. Chem. Res. 38 (1999) 3519.
[34] V. Kasche, B. Galunsky, in: T. Gribnau, J. Visser (Eds.), Affinity Chromatography, Vol. IV, Elsevier–North Holland, Amsterdam, 1982.
[35] N. Gottschlich, V. Kasche, J. Chromatogr. A 765 (1997) 201.
[36] N. Gottschlich, Thesis, TU, Hamburg–Harburg, 1998.
[37] E. Glueckauf, Faraday Soc. Trans. 51 (1955) 1541.
[38] C.H. Liaw, J.S.P. Wang, R.A. Greenkorn, K.C. Chao, AIChE J. 25 (1979) 376.
[39] F.G. Helfferich, Y.-L. Hwang, in: K. Dorfner (Ed.), Ion Exchangers, W. de Gruyter, Berlin, 1991, p. 1285.
[40] H.K. Teoh, M. Turner, N. Titchener-Hooker, E. Sorensen, Comp. Chem. Eng. 25 (2001) 893.
[41] M. Kaspereit, P. Jandera, M. Skavrada, A. Seidel-Morgenstern, J. Chromatogr. A 944 (2002) 249.
[42] E. Wicke, Kolloid-Z. 93 (1940) 129.
[43] S. Yamamoto, Y. Sano, J. Chromatogr. 597 (1992) 173.